N 3 O 6 versus N 2 O 6 coordinated dysprosium slow magnetic relaxation in a tetrathiafulvalene-based dinuclear complex

Olivier Galangau, V. Montigaud, J. Flores Gonzalez, B. Lefeuvre, V. Dorcet, Boris Le Guennic, O. Cador, L. Ouahab, Fabrice Pointillart

N_3O_6 *versus* N_2O_6 Coordinated Dysprosium Slow Magnetic Relaxation in a Tetrathiafulvalene-Based Dinuclear Complex

Olivier Galangau,[a] Vincent Montigaud,[a] Jessica Flores Gonzalez,[a] Bertrand Lefeuvre,[a] Vincent Dorcet,[a] Boris Le Guennic,[a] Olivier Cador,[a] Lahcène Ouahab,[a] Fabrice Pointillart,*[a]

[a] *Univ Rennes, CNRS, ISCR (Institut des Sciences Chimiques de Rennes) - UMR 6226, 35000 Rennes, France*

Corresponding author's email: fabrice.pointillart@univ-rennes1.fr

Dedicated to Professor Miguel Julve on the occasion of his 65th birthday, and for its outstanding contribution to the field of coordination chemistry and molecular magnetism.

Abstract

The reaction between the 2-(1-(4'-[4-(methylphenyl]-2,2:6',2''-terpyridyl)-4,5-(4,5-bis(propylthio)-tetrathiafulvalenyl)-1H-benzimidazol-2-yl)-pyridine (L) and 2 equivalents of $Dy(hfac)_3{\cdot}2H_2O$ ($hfac^-$ = 1,1,1,5,5,5-hexafluoroacetyacetonate) metallic precursors leads to the formation of a dinuclear complex of formula $[Dy_2(hfac)_6(L)]{\cdot}C_6H_{14}$ (Dy2). The X-ray structure on single crystal reveals the occupation of the two benzoimidazolylpyridine (bzip) and terpyridyl (terpy) coordination sites with a Dy(III) ion. The two D_{4d} and C_{4v} Dy(III) ions highlighted slow magnetic relaxation under an applied magnetic field. Even if the two lanthanide centers have similar magnetic anisotropy, they displayed different relaxation times of their magnetization which could be explained by the distinct nature of the magnetic relaxation processes. These conclusions are supported by ab initio calculations.

Keywords: Dysprosium, Tetrathiafulvalene, Single-Molecule Magnet, magnetic relaxation processes, ab initio Calculations

1. Introduction

Lanthanides are the most used metal ions in the design of Single-Molecule Magnets (SMMs) since 15 years[1] because they combine most of the features requested for the observation of slow magnetic relaxation i.e. high magnetic moment and strong magnetic anisotropy.[2] Such magnetic behavior is at the origin of the interest of both chemistry and physics communities because it opens the doors to several potential applications such as high-density data storage,[3] spintronics,[4] quantum computing[5]… The former application implies the observation of high blocking temperature of the systems, temperature at which the magnetic bistability is observed, although it remained limited to very low temperature until very recently.[6] Indeed, the higher level of comprehension of the lanthanide magnetic properties through chemical and symmetry strategies, magneto-structural correlations as well as computational approaches allowed the chemists to rationally design systems[7] to increase the blocking temperature of SMMs close to liquid nitrogen temperature.[8] The blocking temperature of one SMM is now above liquid-nitrogen temperature.[8c]

In our laboratory, the rational design of SMMs is successfully performed by the association of lanthanide ions and redox-active tetrathiafulvalene (TTF)-based ligands.[9] The judicious decoration of the TTF fragments allows the prediction of the architecture of the final coordination compounds. Employing such strategy, mononuclear,[10] dinuclear [11] and auto-assembly of SMM [12] were obtained.

In this article, a novel TTF-based ligand was proposed for which the TTF core is functionalized by both bis-chelating benzoimidazolylpyridine (bzip) and tris-chelating terpyridyl (terpy) coordination pockets. The resulting 2-(1-(4’-[4-(methylphenyl]-2,2:6’,2’’-terpyridyl)-4,5-(4,5-bis(propylthio)-tetrathiafulvalenyl)-1H-benzimidazol-2-yl)-pyridine ligand (**L**) permits the coordination of two Dy(III) ions in N_2O_6 and N_3O_6 environments (Scheme 1). The resulting dinuclear system displays slow magnetic relaxation under an applied magnetic field. A combined experimental and computational analysis led to conclusions about the magnetic anisotropy and relaxation processes for each of the metal centers, explaining the difference of magnetic relaxation times.

2. Experimental Section

2.1. Materials and instrumentations

The precursors $Dy(hfac)_3{\cdot}2H_2O$ ($hfac^-$ = 1,1,1,5,5,5-hexafluoroacetylacetonate anion) was synthesized following previously reported methods [13]. All other reagents were purchased from Aldrich Co., Ltd. and used without further purification.

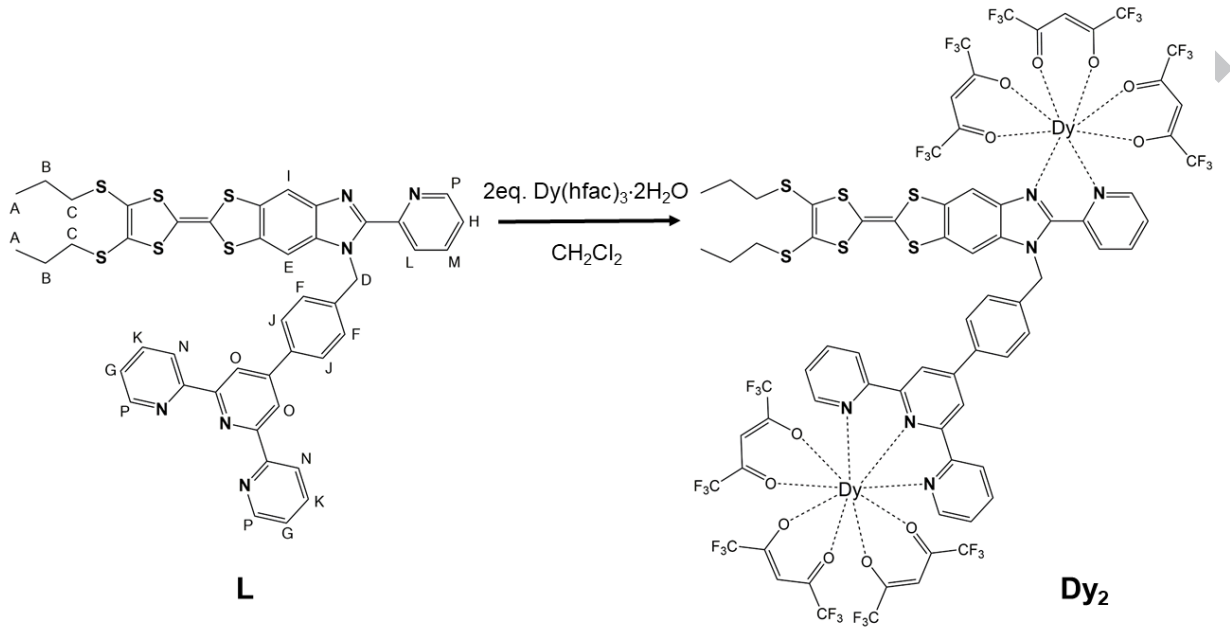

Scheme 1. Synthetic reaction showing the molecular structure of the ligand **L** and labelling scheme for assigning the ^{1}H NMR spectrum as well as the molecular structure of the dinuclear complex $\mathbf{Dy_2}$.

*2.2. Synthesis of the ligand (**L**) and complex ($\mathbf{Dy_2}$)*

*2.2.1. 2-(1-(4'-[4-(methylphenyl]-2,2:6',2''-terpyridyl)-4,5-(4,5-bis(propylthio)-tetrathiafulvalenyl)-1H-benzimidazol-2-yl)-pyridine (**L**).*

2-(4,5-(4,5-bis(propylthio)-tetrathiafulvalenyl)-1*H*-benzimidazol-2-yl)-pyridine[15] (288 mg, 0.555 mmol) and K_2CO_3 (116 mg, 0.841 mmol, 1.5 eq) were added to 5 mL of DMF and then stirred for 30 min under argon. A solution of 2 mL of DMF containing 178 mg of 4'-[4-(bromomethyl)phenyl]-2,2':6',2''-terpyridine[14] (0.443 mmol, 0.8 eq) was added and the resulting mixture was heated at 50°C. After 2h of heating, additional K_2CO_3 (116 mg, 0.841 mmol, 1.5 eq) and 4'-[4-(bromomethyl)phenyl]-2,2':6',2''-terpyridine (89 mg, 0.4 mmol, 0.4 eq) were added. The mixture was stirred and heated overnight at 70°C. The resulting orange solution was cooled down to room temperature leading to the precipitation of an orange powder. The solid was filtered and washed with water (3×50 mL) then with cold methanol and finally dried in air. The orange solid was purified by SiO_2 chromatography with ethyl acetate, pure acetone and then acetone with few drops of acetic acid as eluents giving pure **L**

as yellow powder. Yield 247 mg (53 %). Anal. Calcd (%) for $C_{44}H_{36}N_6S_6$: C 62.86, H 4.29, N 10.00; found: C 62.79, H 4.36 N, 9.91. ^{1}H NMR (CD_2Cl_2): δ 8.69 (m, 3H, P), 8.65 (s, 2H, O), 8.63 (d, 2H, N), 7.62 (td, 1H, M), 8.42 (d, 1H, L), 7.87 (dd, 2H, K), 7.78 (d, 2H, J), 7.69 (s, 1H, I), 7.37 (dd, 1H, H), 7.34 (dd, 2H, G), 7.31 (d, 2H, F), 7.28 (s, 1H, E), 6.21 (s, 2H, D), 2.81 (dt, 4H, C), 1.66 (tt, 4H, B), 1.00 (dd, 6H, A) ppm.

*2.2.2. Complex (**Dy$_2$**)*

[Dy$_2$(hfac)$_6$(L)]·C$_6$H$_{14}$ (Dy$_2$). 32.8 mg of Dy(hfac)$_3$·2H$_2$O (0.04 mmol) were dissolved in 10 mL of CH_2Cl_2 and then added to a solution of 10 mL of CH_2Cl_2 containing 16.8 mg of **L** (0.02 mmol). After 15 minutes of stirring, 25 mL of *n*-hexane were layered at room temperature in the dark. Slow diffusion leads to dark red single crystals which are suitable for X-ray studies. Yield 41 mg (83 %). Anal. Calcd (%) for $C_{80}H_{56}Dy_2F_{36}N_6O_{12}S_6$: C 38.48, H 2.24, N 3.37; found: C 38.40, H 2.29 N, 3.41. I.R. (KBr): 2958 (w), 2928 (w), 2871 (w), 2851 (w), 1652 (s), 1579 (m), 1559 (m), 1533 (m), 1505 (m), 1465 (m), 1413 (m), 1255 (s), 1211 (s), 1145 (s), 1099 (w), 1058 (w), 977 (w), 800 (w), 660 (m) and 585 (w) cm^{-1}.

2.3. X-ray Crystallography.

Single crystals of **L** and **Dy$_2$** were mounted on a APEXIII D8 VENTURE Bruker-AXS diffractometer for data collection (MoK_α radiation source, λ = 0.71073 Å), from the Centre de Diffractométrie (CDIFX), Université de Rennes 1, France. Structures were solved with a direct method using the SHELXT program[15] and refined with a full matrix least-squares method on F^2 using the SHELXL-14/7 program[16]. Crystallographic data are summarized in Table 1. It is worth to notice that the R_1 refinement factor of 11.12% could be explain by the thermal agitation of the "[-terpyDy(hfac)$_3$]" moiety. Complete crystal structure results as a CIF file including bond lengths, angles, and atomic coordinates are deposited as Supporting Information (CCDC 1897266 and 1897267 for **L** and **Dy$_2$** respectively).

2.4. Physical Measurements.

The elementary analyses of the compounds were performed at the Centre Régional de Mesures Physiques de l'Ouest, Rennes. ^{1}H NMR was recorded on a Bruker Ascend 400 spectrometer. Chemical shifts are reported in parts per million referenced to TMS for ^{1}H NMR. Cyclic voltammetry was carried out in CH_2Cl_2 solution, containing 0.1 M $N(C_4H_9)_4PF_6$ as supporting electrolyte. Voltammograms were recorded at 100 mV.s^{-1} at a platinum disk electrode. The potentials were measured *versus* a saturated calomel electrode (SCE). The ac

and dc magnetic susceptibility measurements were performed on solid polycrystalline sample with a Quantum Design MPMS-XL SQUID magnetometer between 2 and 300 K in applied magnetic field of 0.02 T for temperatures of 2-20 K, 0.2 T for temperature of 20-80 K and 1T for temperatures of 80-300 K. These measurements were all corrected for the diamagnetic contribution as calculated with Pascal's constants.

2.4. Computational details.

The atomic positions were extracted from the X-ray crystal structure. To save time and disk space, the CF_3 groups from the $hfac^-$ ligands and the thiopropyl moieties located on the TTF fragment have been replaced by hydrogen atoms leading to the model **Dy_2'** (Fig S1). [17] The optimization of the hydrogen positions, all other atomic positions were kept frozen, has been carried out on the Y(III) parent molecules by Density Functional Theory (DFT) as implemented in the Gaussian 09 (revision D.01) package [18] using the PBE0 hybrid functional. [19][20] The « Stuttgart/Dresden » basis sets and effective core potentials were used to describe the yttrium atom [21] while other atoms were described with the SVP basis sets. [22] Wavefunction-based calculations were carried out on the optimized molecular structure by using the SA-CASSCF/RASSI-SO approach, as implemented in the MOLCAS quantum chemistry package (versions 8.0). [23] In this approach, the relativistic effects are treated in two steps on the basis of the Douglas–Kroll Hamiltonian. First, the scalar terms were included in the basis-set generation and were used to determine the spin-free wavefunctions and energies in the complete active space self-consistent field (CASSCF) method. [24] Next, spin-orbit coupling was added within the restricted-active-space state-interaction (RASSI-SO) method, which uses the spin-free wavefunctions as basis states. [25][26] The resulting spin-orbit wavefunctions and energies are used to compute the static magnetic properties and g-tensors of the lowest states from the energy spectrum by using the pseudospin $\tilde{s} = 1/2$ formalism in the SINGLE_ANISO routine. [27][28] The intramolecular and intermolecular dipolar constants (J_x) are computed using the POLY_ANISO [28][29] routine by building the interaction Hamiltonian on the basis of the ground state doublet of both centers. The overall intermolecular interactions are taken into account by inclusion of a phenomenological parameter (zJ), corresponding to a mean molecular field acting on the magnetic centers, during the simulation of the static magnetic properties. Cholesky decomposition of the bielectronic integrals was employed to save disk space and speed-up the calculations. [30] The active space of the self-consistent field (CASSCF) method consisted of the nine *4f* electrons of the Dy^{III} ion spanning the seven *4f* orbitals, i.e. CAS(9,7)SCF. State-

averaged CASSCF calculations were performed for all of the sextets (21 roots), all of the quadruplets (224 roots), and 300 out of the 490 doublets (due to software limitations) of the Dy(III) ion. 21 sextets, 128 quadruplets, and 107 doublets were mixed through spin−orbit coupling in the RASSI-SO routine. All atoms were described by ANO-RCC basis sets [31-33]. The following contractions were used: [8s7p4d3f2g1h] for Dy atoms, [7s6p4d2f] for Y atoms, [4s3p2d] for O and N atoms, [3s2p] for C atoms, [4s3p] for S atoms and [2s] for H atoms.

To give more insights on the orientation of the anisotropy axes, the molecular electrostatic potential is calculated from the *ab-initio* LOPROP charge analysis [34], using the home-made CAMMEL code (CAlculated Molecular Multipolar ELectrostatics),[35] following:

$$V(r_i) = \sum_{i}^{N} \frac{q_i}{|r_i - r|} + \frac{p_i \cdot r_i}{|r_i - r|^3} + \frac{r_i \cdot (Q_i \times r_i)}{|r_i - r|^5}$$

where q_i,p_i, Q_i are respectively the charge, dipole and quadrupole moments of the i-th atom. The total potential, and its components, are drawn on a sphere defined by the user around the central lanthanide ion. For a clearer representation of the potential, the intensity can be directly related to both the color (red = high potential and blue = low potential) and the height of the irregularities.

3. Results and discussion

3.1. Crystal structures of ***L*** *and* ***Dy$_2$***

*2-(1-(4'-[4-(methylphenyl]-2,2:6',2''-terpyridyl)-4,5-(4,5-bis(propylthio)-tetrathiafulvalenyl)-1H-benzimidazol-2-yl)-pyridine (**L**).*

The ligand **L** crystallizes in the $P2_1/n$ monoclinic space group (Table 1). The asymmetric unit is composed by only one molecule of **L** (Fig. 1). The neutrality of **L** is confirmed by the central C9-C10 bond length of 1.325(7) Å and the boat conformation of the TTF core. The phenyl spacer and the terpy moiety form an angle of 23.5(1)°.

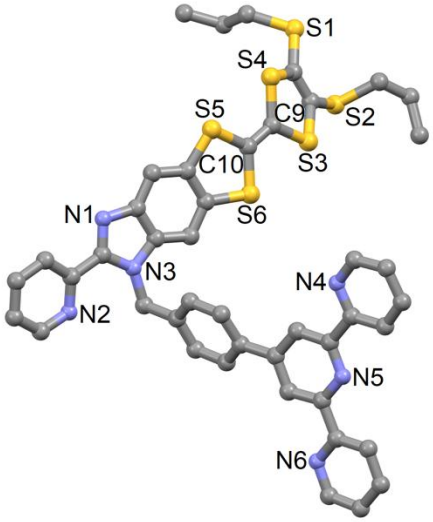

Fig. 1. X-ray structure of **L** with numbering of the heteroatoms. All hydrogen atoms are omitted for clarity.

The crystal packing reveals the formation of "head-to-tail" dimers of **L** through π-π interactions between the terpy moieties along the c axis (Fig 2a.). Along the a axis, regular one-dimensional stacking of TTF fragments through S1···S2 = 3.601 Å, S3···S4 = 3.967 Å and S5···S6 = 3.949 Å contacts and one-dimensional π-π stacking of terpy moieties are identified (Fig. 2b).

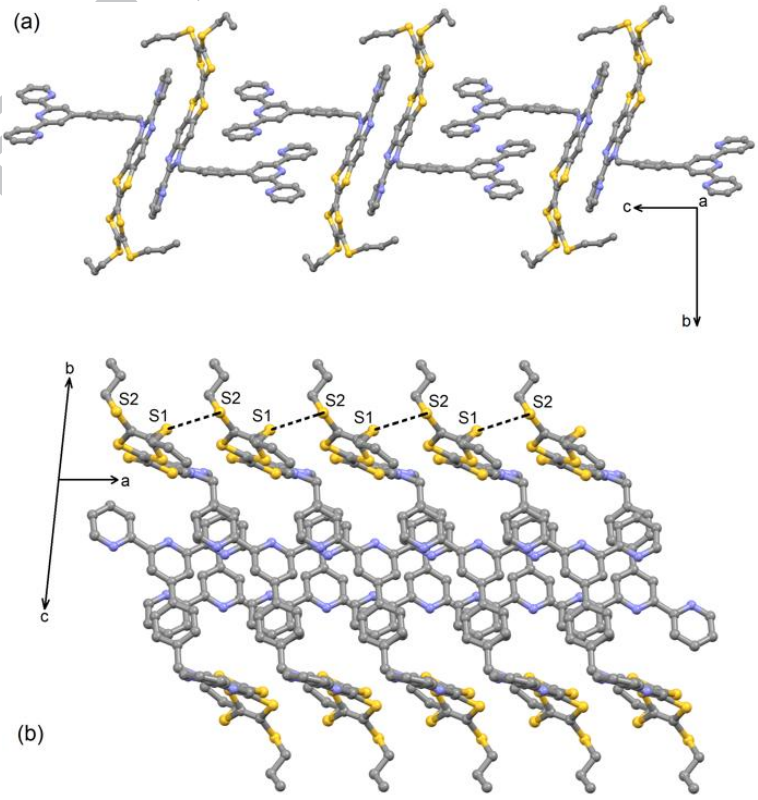

Fig. 2. Crystal packing of **L** along the c (a) and a (b) axes.

Table 1. X-ray crystallographic data for **L** and **Dy_2**.

Compounds	(**L**)	$[Dy_2(hfac)_6(\mathbf{L})]\cdot C_6H_{14}$ (**Dy_2**)
Formula	$C_{44}H_{36}N_6S_6$	$C_{80}H_{56}Dy_2F_{36}N_6O_{12}S_6$
M / g.mol^{-1}	841.15	2494.7
Crystal system	Monoclinic	triclinic
Space group	$P2_1/n$ (N°14)	P-1 (N°2)
Cell parameters	a = 6.6369(8) Å b = 32.290(4) Å c = 18.516(2) Å β = 97.858(5) °	a = 12.7624(15) Å b = 17.362(2) Å c = 22.824(3) Å α = 88.720(4) ° β = 83.473(4) ° γ = 71.130(4) °
Volume / Å^3	3930.9(8)	4754.1(10)
Z	4	2
T / K	150 (2)	150(2)
2θ range /°	5.84 ≤ 2θ ≤ 54.95	5.90 ≤ 2θ ≤ 54.97
ρ_{calc} / g.cm^{-3}	1.421	1.743
μ / mm^{-1}	0.391	1.815
Number of reflections	23402	72434
Independent reflections	8497	20658
R_{int}	0.0864	0.0872
$Fo^2 > 2\sigma(Fo)^2$	5689	13602
Number of variables	505	864
R_1, wR_2	0.0967, 0.1830	0.1112, 0.3061

$[Dy_2(hfac)_6(\mathbf{L})]\cdot C_6H_{14}$ (**Dy_2**). Compound **Dy_2** crystallizes in the P-1 (N°2) triclinic space group (Table 1). The asymmetric unit is composed of two $Dy(hfac)_3$ moieties, one **L** ligand, and one *n*-hexane molecule of crystallization (Fig. 3). The two bzip and terpy moieties of **L** coordinated one $Dy(hfac)_3$ unit each. Thus, the Dy1 ion is surrounded by six oxygen atoms that belong to three $hfac^-$ ligands and two nitrogen atoms coming from the bis-chelating coordination site (bzip) of **L**. The averaged Dy1-O (2.327(8) Å) and Dy1-N (2.513(10) Å) distances are in the same range than those already observed for a Dy(III) ion in similar environment. [10a] [10c] [11b] [11c] [36] A square antiprism coordination polyhedron (D_{4d} symmetry) is induced by the arrangement of the ligands around the Dy1 (Table 2). The distortion is visualized by continuous shape analysis performed with SHAPE 2.1. [37] The Dy2 ion is surrounded by six oxygen atoms that belong to three $hfac^-$ ligands and three nitrogen atoms coming from the tris-chelating coordination site (terpy). Once again, the

averaged Dy2-O distance is slightly longer (2.372(18) Å) than for Dy1-O while the averaged Dy2-N distance (2.493(16) Å) is shorter than for Dy1-N. Such variation could be assigned to the difference of steric hindrance between the two coordination sites. The best symmetry describing the coordination polyhedron around Dy2 is capped square antiprism (C_{4v}) (Table 2). It is worth to notice that the tris-chelating coordination site 2,6-di(pyrazol-1-yl)-4-pyridine (dpp) induced a D_{3h} symmetry. [11b] [36]

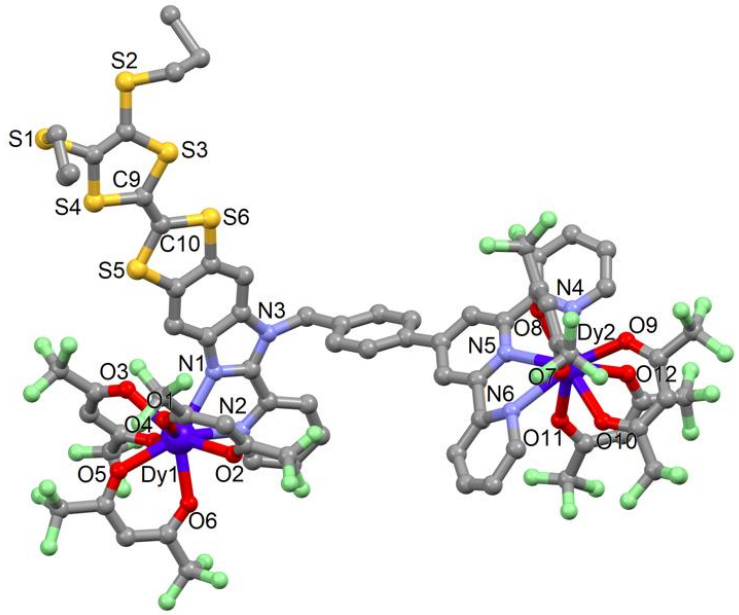

Fig. 3. Molecular structure of the dinuclear complex $[Dy_2(hfac)_6(\mathbf{L})]\cdot C_6H_{14}$ (**Dy_2**). Hydrogen atoms and crystallization solvent molecules are omitted for clarity.

Table 2. SHAPE analysis of the coordination polyhedra around each lanthanide center of **Dy_2**.

Metal	$CShM_{SAPR-8}$ (square antiprism D_{4d})	$CShM_{BTPR-8}$ (biaugmented trigonal prism C_{2v})	$CShM_{TDD-8}$ (triangular dodecahedron D_{2d})	$CShM_{TCTPR-9}$ (spherical tricapped trigonal prism D_{3h})	$CShM_{CSAPR-9}$ (spherical capped square antiprism C_{4v})	$CShM_{MFF-9}$ (Muffin)
Dy1	0.521	1.845	1.812	/	/	/
Dy2	/	/	/	1.509	1.087	1.231

The central C=C bond distance of the TTF core is equal to 1.325(18) Å confirming the neutral form of **Dy_2**. The two planes formed by the bzip and phenyl spacer are nearly perpendicular. The angle between this same phenyl spacer and the plane formed by the terpy moiety increases from 23.5(1)° to 35.2(4)° after coordination with the Dy(III) precursors. The intramolecular Dy-Dy distance is found equal to 14.563 Å which is much longer than the shortest intermolecular Dy1-Dy1 distance (8.368 Å). The crystal packing highlighted the formation of isolated "head-to-tail" dimers of **Dy_2** through π-π stacking of **L** (Fig. 4). Consequently, no S···S contacts are identified in the crystal structure.

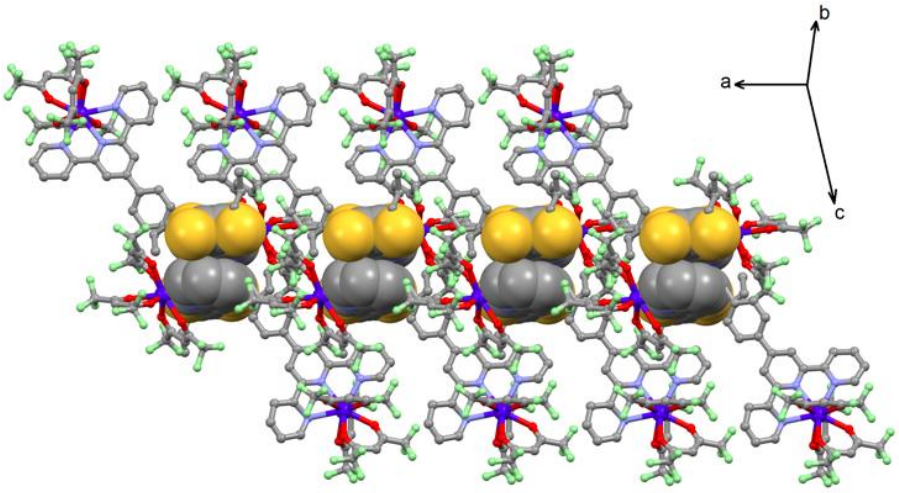

Fig. 4. Crystal packing of **Dy_2** highlighting the formation of dimers of **L**.

3.2. Electrochemical Properties.

The redox properties of **L** and the related complex **Dy_2** are investigated by cyclic voltammetry (Fig. 5) and the values of the oxidation potentials are listed in Table 3.

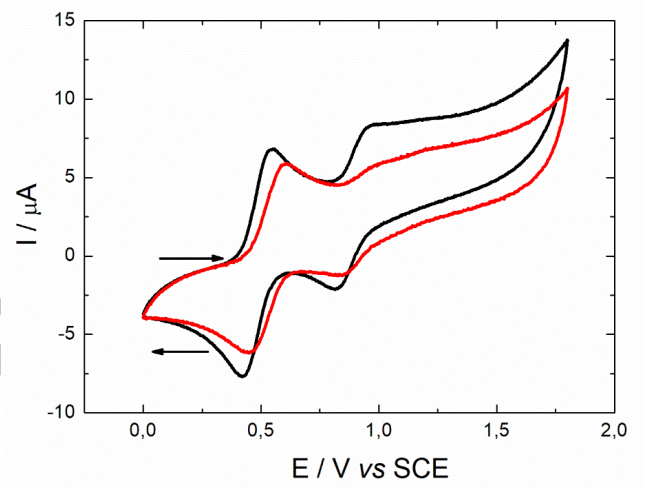

Fig. 5. Cyclic voltammograms of **L** (black line) and $[Dy_2(hfac)_6(\mathbf{L})]\cdot C_6H_{14}$ (red line) in CH_2Cl_2 at a scan rate of 100 $mV\cdot s^{-1}$. The potentials were measured *vs*. a saturated calomel electrode (SCE) with Pt wires as working and counter electrodes.

Table 3. Oxidation potentials (V *vs* SCE, nBu_4NPF_6, 0.1 M in CH_2Cl_2 at 100 $mV.s^{-1}$) of **L** and **Dy_2**.

	$E^1_{1/2}$ / V		$E^2_{1/2}$ / V	
	$^{Ox}E^1$	$^{Red}E^1$	$^{Ox}E^2$	$^{Red}E^2$
L	0.55	0.42	0.97	0.81
Dy_2	0.61	0.45	1.00	0.85

The cyclic voltammogram of **L** shows two one-electron oxidations at about 0.49 V and 0.89 V corresponding to the formation of a radical cation and a dication TTF fragment, respectively (Fig. 5). [38] These oxidation potentials are the same to those found for the functionalized TTF involving the molecular skeleton 4,5-bis(propylthio)-tetrathiafulvalenyl]-1*H*-benzimidazol-2-yl}pyridine [37], demonstrating that the nature of the alkylating group has no influence on the electrochemical properties, as expected. Upon coordination of the lanthanide, the electrochemistry highlighted only weak effect of the electron attracting $Dy(hfac)_3$ fragments with a slight shift of the oxidation-reduction waves to higher potentials (+0.04 V) (Table 3). The reversibility of the oxidation potentials is preserved and the electrochemical properties attest the redox-activity of **L** in the complex. These results suggest that complex **Dy_2** would be a suitable candidate for redox controlled magnetometric measurements.

3.3. Magnetic Properties.

Static measurements.

The temperature dependence of the $\chi_M T$ product for compound **Dy_2** is represented on Fig. 6. The system exhibits a room temperature value of 27.83 cm^3 K mol^{-1}, close to the expected value for two isolated Dy(III) ions with ground state multiplets $^6H_{15/2}$ with $g_J = 4/3$ (i.e. 28.4 cm^3 K mol^{-1}). [39]

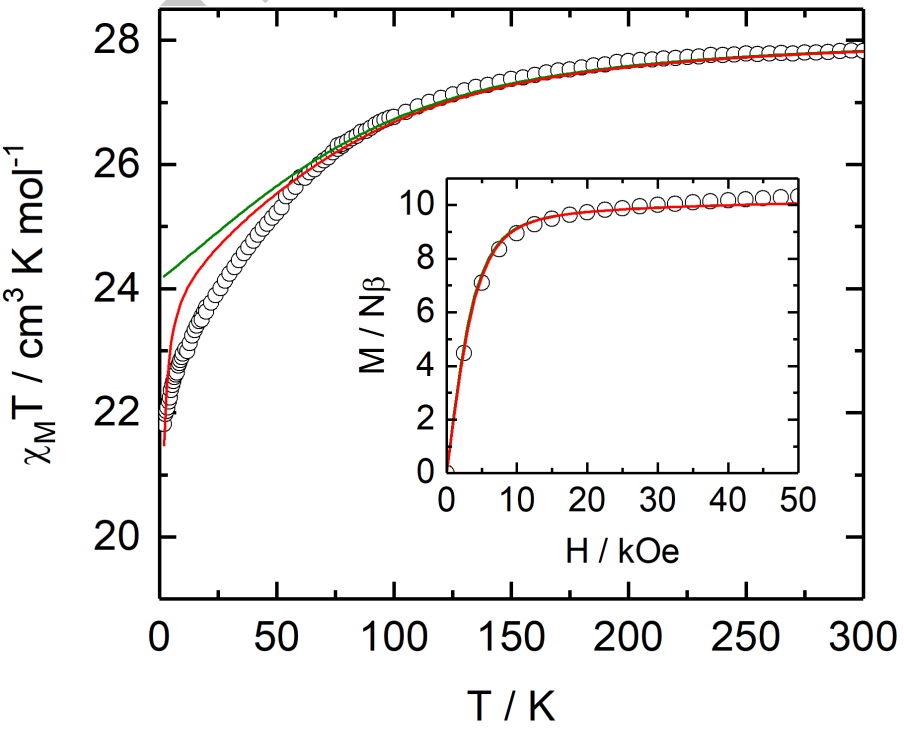

Fig. 6. Thermal dependence of $\chi_M T$ for **Dy_2**. Inset: field variation of the magnetization measured at 2 K. Full colored lines correspond to the simulated ab initio curves: green curves correspond to isolated magnetic centers while red curves stand for the addition of antiferromagnetic intermolecular interactions ($zJ = -0.03$ cm^{-1}).

Upon cooling, the thermal depopulation of the ligand field sublevels leads to a monotonic decrease of the $\chi_M T$ product which reaches the value of 21.82 cm^3 K mol^{-1} at the lowest temperature (2K). The field-dependence of the magnetization measured at 2 K is depicted in inset of Fig. 6. At 5 T, the value of the magnetization reaches 10.32 μ_B which is far from the expected saturated values of 20 μ_B for two Dy(III).

Dynamic measurements.

The out-of-phase component of the ac susceptibility (χ_M'') for **Dy_2** was measured using immobilized crushed single crystals. Under zero applied magnetic field, an out-of-phase signal was detected at the highest frequency at 2 K but no maximum could be observed. The fast magnetic relaxation could be attributed to the quantum tunneling of the magnetization (QTM) process and in order to cancel it, a field dependence of the magnetic susceptibility is studied. The application of a magnetic field led to the appearance of an out-of-phase component of the magnetic susceptibility. Nevertheless, two contributions are observed whatever the value of the magnetic field (Figs. 7, S2 and S3) and the value of 3000 Oe is selected (value at which the two relaxation contributions are both at the lowest frequency and clearly identified). The frequencies maxima were manually selected to plot the temperature dependence of the relaxation time ($\log(\tau)$ vs T for both high (red plots) and low frequency (black plots) contributions (Fig. 8).

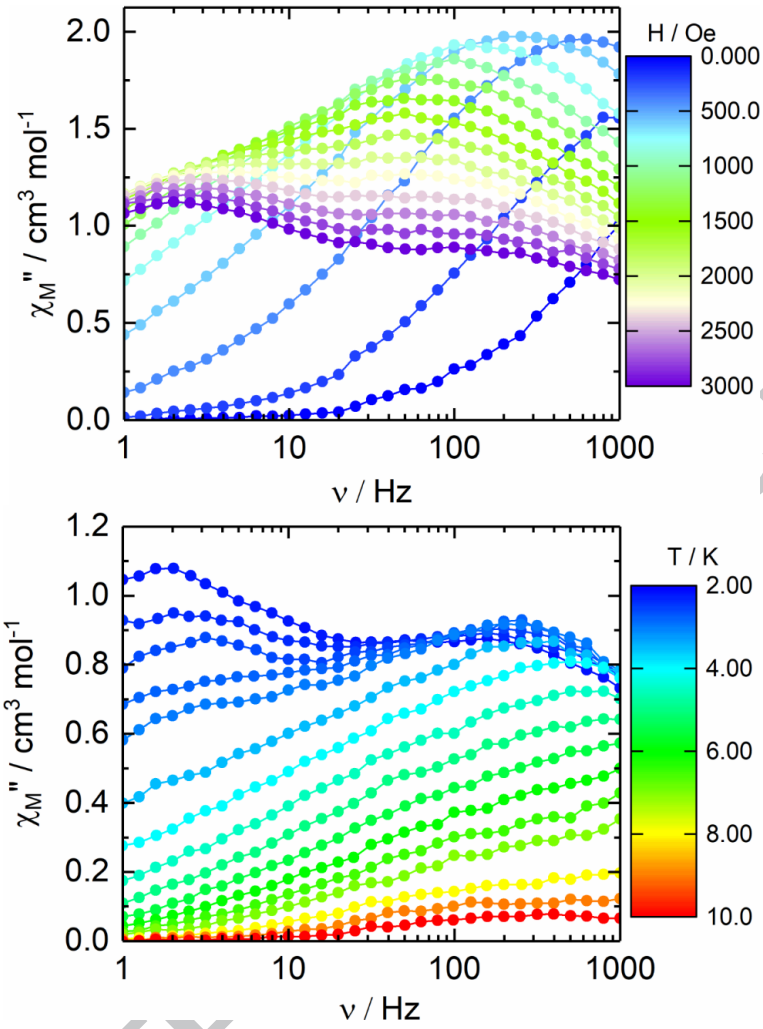

Fig. 7. Frequency dependence of the out-of phase, χ_M'', component of the magnetic susceptibility at 2 K at various external dc field (top). Frequency dependence of χ_M'' between 2 and 10 K for **Dy_2** at 3000 Oe (bottom).

Based on our previous studies, the low and high frequency contributions can be attributed to the Dy(III) ions in N_2O_6 (Dy1) and N_3O_6 (Dy2) environments respectively. [11b] Indeed, some of us have evidenced that the N_2O_6 environment, [10] identical to the one of this work, favor slow relaxation in zero external field while the slow relaxation in N_3O_6 environment only shows up in external field [11b].

Attempts to extract energy barriers from the Arrhenius plot led to very small values compared to the calculated ones (see below) leading to the exclusion of the sole Orbach process. [40] The thermal dependence of the Arrhenius law under an applied magnetic field can be fitted taking into account both Raman and Direct processes ($\tau^{-1} = CT^n + AT$). This does not mean that Orbach process is not involved but that it is much slower than the Raman and Direct. The best fits were obtained considering the following parameters: C = 0.14(3) $s^{-1}K^{-n}$, n = 4.20(12)

and A = 3.0(5) $Oe^{-m}s^{-1}K^{-1}$ for Dy1 (where m is fixed to 4) and C = 3.87(3) $s^{-1}K^{-n}$, n = 4.34(55) and A = 381(37) $Oe^{-m}s^{-1}K^{-1}$ for Dy2 (where m is fixed to 4) (Fig. 8). Values of n close to 9 are expected for Kramers ions but they can decrease down to 4 depending of the energies of the ground state doublets.[41] From these fits, one could conclude that Dy1 seems to relax mainly through a Raman process while, for Dy2, the main magnetic relaxation process is a Direct mechanism with a Raman contribution. Such process of relaxation for Dy1 is in agreement with what some of us already observed for a Dy(III) in D_{4d} N_2O_6 environment while the weak contribution of the Direct process comes from the 3000 Oe applied magnetic field instead of the optimal 1000 Oe for isolated Dy(III) in such surrounding. [10c]

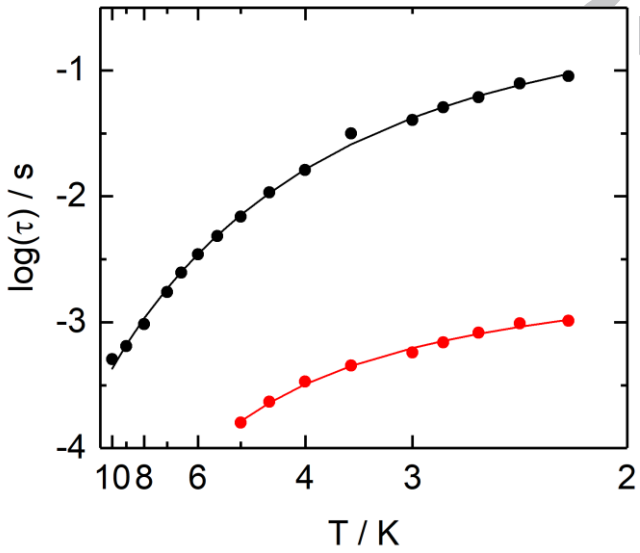

Fig. 8. Temperature dependences of the relaxation times (τ) at 3000 Oe for **Dy_2** in the temperature range 2-10 K for Dy1 (black plots) and 2-5 K for Dy2 (red plots). Black and red lines are the best fitted curves with parameters given in the text.

Ab initio calculations.

The experimental magnetic properties are rationalized by SA-CASSCF/RASSI-SO calculations on a truncated version of **Dy_2,** referred as **Dy_2'** (see computational details and Fig S1). A calculation is performed for each Dy(III) center present in the model dimer unit **Dy_2'**, namely Dy1 and Dy2. Despite the strong differences in coordination sphere nature and geometry between the two magnetic centers, the calculations show similar ground state properties. In both cases, the ground state is characterized by a strongly uniaxial (Ising-type) magnetic anisotropy, g_Z = 19.61 and 19.68 (with gx and gy close to zero) for Dy1 and Dy2 respectively, reflecting an almost pure M_J=|±15/2> Stark sublevel (Tables S1 and S2). The orientation of the computed easy axes tends to follow the most negatively charged O atoms

from the $hfac^-$ ligands, perpendicular to the plane containing the N atoms from the bis-chelating and tris-chelating pockets of **L** (Fig. 9a) and leading to an angle of 64.6° between the two magnetic axes. This is further supported by plotting the molecular electrostatic potential around each Dy(III) center, using the home-made software CAMMEL. This representation highlights the larger distribution of the potential along the O atoms from the $hfac^-$ ligands (Fig. 9b, 9c). The decomposition of the total electrostatic potential into the charge, dipole and quadrupole contributions emphasizes the major contribution of the quadrupole term to the total potential, as already observed for Dy(III) systems (Figs. S4, S5).[10c][35][42] The computation of the relaxation barriers for each non-equivalent center tends to highlight a thermally-assisted QTM mechanism occurring through the third excited state and leading to a calculated energy barrier of 207 cm^{-1} for Dy1 (Fig. S6). On the contrary, the large coefficient between the ground and first excited state observed for Dy2 seems to favor an Orbach process involving the first excited state with a barrier of 178 cm^{-1} (Fig. S7). At this point, the calculations underline the similar properties of both Dy(III) centers in terms of magnetic anisotropy and ground state properties regardless the coordination sphere nature and geometry. However, differences in the local environments of the lanthanide centers induced strong variations of the ligand field leading to distinct relaxation mechanisms for both centers.

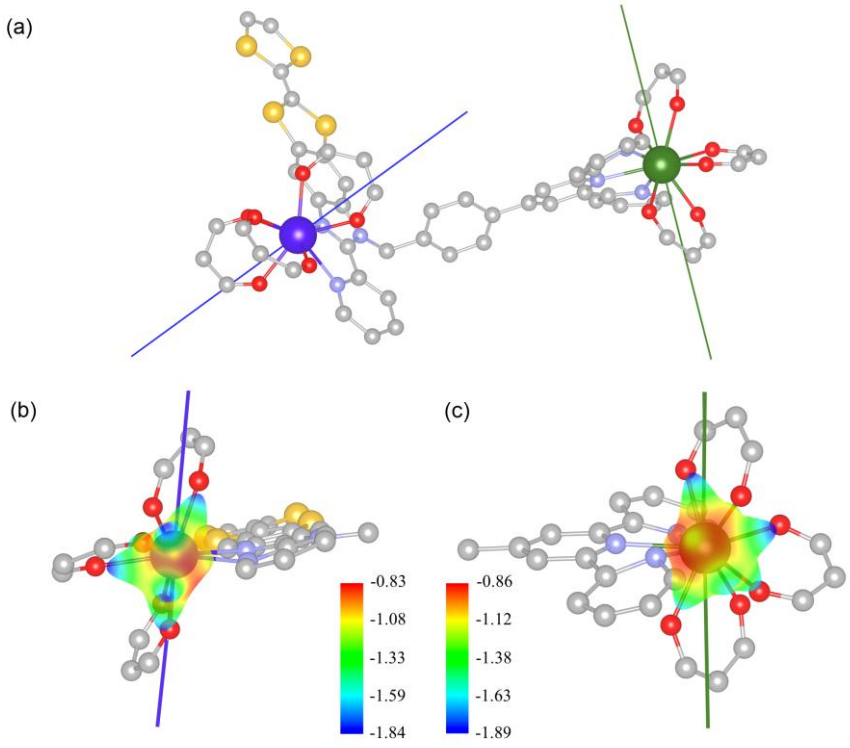

Fig. 9. Orientations of the ground state g-tensor main component (g_z) computed for **Dy_2'** (a) and projection of the molecular potential on Dy1 (b, blue line) and Dy2 (c, green line) centers.

A first attempt to describe the static magnetic properties by considering non-interacting magnetic centers lead to a good description of the high-temperature region of both the $\chi_M T$ product and the field dependence of the magnetization but failed to reproduce the decrease observed in the low-temperature range of the magnetic susceptibility (Fig. 6). Based on the orientation of the ground state magnetic axes and the large Dy1-Dy2 distance, intramolecular magnetic interactions were considered negligible (J_{intra} = 0.002 cm^{-1}). However, the presence of shorter Dy-Dy distances in the crystal tends to favor intermolecular dipolar interactions. Moreover, the heterogeneous distribution of these distances, around Dy1 and Dy2, creates inequivalent magnetic environments (Fig. S8). These environments are modeled by considering the first magnetic neighbors within a sphere with a radius of 12 Å around the central Dy1/Dy2 ions. Each asymmetric center exhibits two types of magnetic interactions referred as Dy1-Dy1 (Dy2-Dy2) and Dy1-Dy2 interactions. The computation (within the $\tilde{s} = {}^1/_2$ approximation) of the dipolar constants, J_X, corresponding to each interacting pair (Fig. S8 and Table S3), attests the weakness of these interactions (10^{-2}-10^{-3} cm^{-1}), which is mainly due to the large Dy-Dy distances observed in the crystal. The calculated J_X values highlights the antiferromagnetic character ($J_X < 0$) of Dy1-Dy1 and Dy2-Dy2 interactions and the ferromagnetic character ($J_X > 0$) of Dy1-Dy2 interactions. Based on these results, and in order to increase the description of the system and to fit the experimental data, the effect of this magnetic environment was studied through the incorporation of a phenomenological parameter (zJ) in the calculations. The best agreement with experimental data was found for an effective antiferromagnetic field of zJ=-0.03 cm^{-1} (Fig. 6), in agreement with the values found for the local magnetic environments.

4. Conclusions

A novel TTF-based ligand (**L**) was designed with two available terpyridine (terpy) and benzoimidazol-2-pyridine (bzip) coordination sites. This ligand allows the formation of a dinuclear compound of formula $[Dy_2(hfac)_6(\mathbf{L})]\cdot C_6H_{14}$ (**Dy_2**) in which the Dy(III) are in D_{4d} N_2O_6 and C_{4v} N_3O_6 environments. **Dy_2** behaves as a field-induced Single-Molecule Magnet with two distinct magnetic relaxation times. The N_2O_6 Dy1 magnetization relaxes slower than the one of the N_3O_6 Dy2. A*b initio* calculations highlighted similar ground states properties

(almost pure $M_J = \pm 15/2$, $g_z \sim 20$) for both Dy(III) ions. However, the strong variation of the ligand field between Dy1 and Dy2, arising from the two different coordination spheres, results in two distinct relaxation mechanisms. The computational results emphasize a complicated relaxation mechanism in Dy1, involving several excited states and explaining the longer relaxation time observed, when compared to Dy2 which tends to relax through the first excited state. The description of the local magnetic environment of each asymmetric Dy(III) ion highlighted weak intramolecular and intermolecular magnetic interactions occurring in the crystal. The decomposition of these interactions revealed the presence of both antiferromagnetic (between equivalent centers) and ferromagnetic (between non-equivalent centers) contributions.

The ligand **L** is chemically suitable to build heterobimetallic complexes to incorporate additional physical properties such as luminescence and Spin crossover, and the influence of one of the metal center on the properties of the other one is in progress in our laboratory.

Acknowledgments. This work was supported by Région Bretagne, Rennes Métropole, CNRS, Université de Rennes 1 and the European Commission through the ERC-CoG 725184 MULTIPROSMM (project n. 725184). B.L.G. and V.M. thank the French GENCI/IDRIS-CINES center for high-performance computing resources.

Appendix A. Supplementary data: CCDC 1897266 and 1897267 contains the supplementary crystallographic data for **L** and **Dy_2**, respectively. Computational models (Fig. S1), Frequency dependence of χ_M' for **Dy_2** at 2 K between 0-3000 Oe (Fig. S2) and frequency dependences of χ_M' for **Dy_2** in applied field (Fig. S3). Decomposition of the molecular electrostatic potential into the charge, dipolar and quadrupolar components for each Dy(III) centers in **Dy_2** (Figs. S4 and S5). Magnetization blocking barrier for each Dy(III) centers in **Dy_2** (Figs. S6 and S7). Representation of the magnetic environments around the two Dy(III) centers in **Dy_2** corresponding to the first magnetic neighbors (Fig. S8).

References

[1] N. Ishikawa, M. Sugita, T. Ishikawa, S. Y. Koshihara, Y. Kaizu, J. Am. Chem. Soc. 125 (2003) 8694.

[2] D. N. Woodruff, R. E. P. Winpenny, R. A. Layfield, Chem. Rev. 113 (2013) 5110.

[3] M. Mannini, F. Pineider, P. Sainctavit, C. Danieli, E. Otero, C. Sciancalepore, A. M. Talarico, M.-A. Arrio, A. Cornia, D. Gatteschi, R. Sessoli, Nat. Mater. 8 (2009) 194.

[4] (a) K. S. Pedersen, A.-M. Ariciu, S. McAdams, H. Weihe, J. Bendix, F. Tuna, S. Piligkos, J. Am. Chem. Soc. 138 (2016) 5801; (b) L. Bogani, W. Wernsdorfer, Nature Mater. 7 (2008) 179; (c) J. Lehmann, A. Gaita-Arino, E. Coronado, D. Loss, Nature Nanotech. 2 (2007) 312; (d) M. Ganzhorn, S. Klyatskaya, M. Ruben, W. Wernsdorfer, Nature Nanotech. 8 (2013) 165.

[5] (a) S. Thiele, F. Balestro, R. Ballou, S. Klyatskaya, M. Ruben, W. Wernsdorfer, Science 344 (2014) 1135; (b) M. N. Leuenberger, D. Loss, Nature 410 (2001) 789.

[6] (a) M. Gregson, N. F. Chilton, A.-M. Ariciu, F. Tuna, I. F. Crowe, W. Lewis, A. J. Blake, D. Collison, E. J. L. McInnes, R. E. P. Winpenny, S. T. Liddle, Chem. Sci. 2016, 7, 155; (b) J. D. Rinehart, M. Fang, W. J. Evans, J. R. Long, J. Am. Chem. Soc. 133 (2011), 14236; (c) J. D. Rinehart, M. Fang, W. J. Evans, J. R. Long, Nat. Chem. 3 (2011) 538; (d) S.-D. Jiang, B.-W. Wang, H.-L. Sun, Z.-M. Wang, S. Gao, J. Am. Chem. Soc. 133 (2011) 4730; (e) M. Gonidec, E. S. Davies, J. McMaster, D. B. Amabilino, J. Veciana J. Am. Chem. Soc. 132 (2010) 1756; (f) F. Habib, P.-H. Lin, J. Long, I. Korobkov, W. Wernsdorfer, M. Murugesu 133 (2011) 8830; (g) Y.-N. Guo, G.-F. Xu, W. Werndorfer, L. Ungur, Y. Guo, J. Tang, H.-J. Zhanf, L. F. Chibotaru, A. K. Powell J. Am. Chem. Soc. 133 (2011) 11948; (h) T. P. Latendresse, N. S. Bhuvanesh, M. Nippe 139 (2017) 8058; (i) J. Liu, Y.-C. Chen, J.-L. Liu, V. Vieru, L. Ungur, J.-H. Jia, L. F. Chibotaru, Y. Lan, W. Wernsdorfer, S. Gao, X.-M. Chen, M.-L. Tong J. Am. Chem. Soc. 138 (2016) 5441.

[7] (a) G. Cucinotta, M. Perfetti, J. Luzon, M. Etienne, P. E. Car, A. Caneschi, G. Calvez, K. Bernot and R. Sessoli, *Angew. Chem. Int. Ed.* 51 (2012)1606; (b) J. Long, R. Vallat, R. A. S. Ferreira, L. D. Carlos, F. A. A. Paz, Y. Guari and J. Larionova, *Chem. Commun.*, 48 (2012)9974; (c) K. Yamashita, R. Miyazaki, Y. Kataoka, T. Nakanishi, Y. Hasegawa, M. Nakano, T. Yamamura and T. Kajiwara, *Dalton Trans.*, 42 (2013) 1987; (d) K. Ehama, Y. Ohmichi, S. Sakamoto, T. Fujinami, N. Matsumoto, N. Mochida, T. Ishida, Y. Sunatsuki, M. Tsuchimoto and N. Re, *Inorg. Chem.* 52 (2013) 12828; (e) M. Ren, S.-S. Bao, R. A. S. Ferreira, L.-M. Zheng and L. D. Carlos, *Chem. Commun.*, 50 (2014) 7621; (f) X. Yi, K. Bernot, V. Le Corre, G. Calvez, F. Pointillart, O. Cador, B. Le Guennic, J. Jung, O. Maury, V. Placide, Y. Guyot, T. Roisnel, C. Daiguebonne and O. Guillou, *Chem. Eur. J.*, 20 (2014) 1569; (g) G. Cosquer, F. Pointillart, J. Jung, B. Le Guennic, S. Golhen, O. Cador, Y. Guyot, A. Brenier, O. Maury, L. Ouahab, Eur. J. Inorg. Chem. (2014) 69; (h) F. Pointillart, B. Le

Guennic, S. Golhen, O. Cador, O. Maury, L. Ouahab, Chem. Commun. 49 (2013) 615; (i) J. Long, Y. Guari, R. A. S. Ferreira, L. D. Carlos, J. Larionova, Coord. Chem. Rev. 363 (2018) 57; (j) Y. S. Meng, S.-D. Jiang, B.-W. Wang, S. Gao, Acc. Chem. Res. 49 (2016) 2381; (k) S. T. Liddle, J. Van Slageren, Chem. Soc. Rev. 44 (2015) 6655; (l) J.-L. Liu, Y.-C. Chen, M.-L. Tong, Chem. Soc. Rev. 47 (2018) 2431; (m) Z. Zhu, M. Guo, X.-L. Li, J. Tang, Coord. Chem. Rev. 378 (2019) 350.

[8] F.-S. Guo, B.-M. Day, Y.-C. Chen, M.-L. Tong, A. Mansikkamäki, R. A. Layfield, Angew. Chem., Int. Ed. 56 (2017) 11445; (b) C. A. P. Goodwin, F. Ortu, D. Reta, N. F. Chilton, D. P. Mills, Nature 548 (2017) 439; (c) K. R. McClain, C. A. Gould, K. Chakarawet, S. J. Teat, T. J. Groshens, J. R. Long, B. G. Harvey, Chem. Sci. 9 (2018) 8492; F.-S. Guo, B.-M. Day, Y.-C. Chen, M.-L. Tong, A. Mansikkamäki, R. A. Layfield, Science 362 (2018) 1400.

[9] F. Pointillart, B. Le Guennic, O. Cador, O. Maury, L. Ouahab, Acc. Chem. Res. 48 (2015) 2834.

[10] (a) G. Cosquer, F. Pointillart, S. Golhen, O. Cador, L. Ouahab, Chem. Eur. J. 19 (2013) 7895 (b) T. T. da Cunha, J. Jung, M.-E. Boulon, G. Campo, F. Pointillart, C. L. M. Pereira, B. Le Guennic, O. Cador, K. Bernot, F. Pineider, S. Golhen, L. Ouahab, J. Am. Chem. Soc. 135 (2013) 16332; (c) F. Pointillart, J.-K. Ou-Yang, G. Fernandez-Garcia, V. Montigaud, J. Flores Gonzalez, R. Marchal, L. Favereau, F. Totti, J. Crassous, O. Cador, L. Ouahab, B. Le Guennic, Inorg. Chem. 58 (2019), 52.

[11] (a) F. Pointillart, Y. Le Gal, S. Golhen, O. Cador, L. Ouahab, Chem. Eur. J. 17 (2011) 10397 ; (b) M. Feng, F. Pointillart, B. Lefeuvre, V. Dorcet, S. Golhen, O. Cador, L. Ouahab, Inorg. Chem. 54 (2015), 4021; (c) S. Speed, M. Feng, G. Fernandez-Garcia, F. Pointillart, B. Lefeuvre, F. Riobé, S. Golhen, B. Le Guennic, F. Totti, Y. Guyot, O. Cador, O. Maury, L. Ouahab, Inorg. Chem. Front, 4 (2017) 604.

[12] F. Pointillart, T. Guizouarn, B. Lefeuvre, S. Golhen, O. Cador, L. Ouahab, Chem. Eur. J. 21 (2015) 16929.

[13] M. F. Richardson, W. F. Wagner, D. E. Sands, J. Inorg. Nucl. Chem. 30 (1968) 1275.

[14] A. Paul, A. P. C. Ribeiro, A. Karmakar, M. Fatima C. Guedes da Silva, A. J. L. Pombeiro, Dalton Trans. 45 (2016) 12779.

[15] G. L. Sheldrick, Acta Crystallogr., Sect. A Found Adv. 71 (2015) 3.

[16] G. M. Sheldrick, Acta Crystallogr. Sect. C 71 (2015) 3.

[17] F. Habib, G. Brunet, V. Vieru, I. Korobkov, L. F. Chibotaru, M. Murugesu, J. Am. Chem. Soc. 135 (2013) 13242.

[18] M. J. Frisch, G. W. Trucks, H. B. Schlegel, G. E. Scuseria, M. A. Robb, J. R. Cheeseman, G. Scalmani, V. Barone, B. Mennucci, G. A. Petersson, H. Nakatsuji, M. Caricato, X. Li, H. P. Hratchian, A. F. Izmaylov, J. Bloino, G. Zheng, J. L. Sonnenberg, M. Hada, M. Ehara, K. Toyota, R. Fukuda, J. Hasegawa, M. Ishida, T. Nakajima, Y. Honda, O. Kitao, H. Nakai, T. Vreven Jr., J. A. Montgomery, J. E. Peralta, F. Ogliaro, M. Bearpark, J. J. Heyd, E. Brothers, K. N. Kudin, V. N. Staroverov, R. Kobayashi, J. Normand, K. Raghavachari, A. Rendell, J. C. Burant, S. S. Iyengar, J. Tomasi, M. Cossi, N. Rega, J. M. Millam, M. Klene, J. E. Knox, J. B. Cross, V. Bakken, C. Adamo, J. Jaramillo, R. Gomperts, R. E. Stratmann, O. Yazyev, A. J. Austin, R. Cammi, C. Pomelli, J. W. Ochterski, R. L. Martin, K. Morokuma, V. G. Zakrzewski, G. A. Voth, P. Salvador, J. J. Dannenberg, S. Dapprich, A. D. Daniels, O. Farkas, J. B. Foresman, J. V. Ortiz, J. Cioslowski and D. J. Fox, Gaussian 09 Revision D.01, Gaussian Inc.: Wallingford, CT, USA, 2013.

[19] J. P. Perdew. K. Burke. M. Ernzerhof, Phys. Rev. Lett. 77 (1996) 3865.

[20] C. Adamo. V. Barone, J. Chem. Phys. 110 (1999) 6158.

[21] M. Dolg. H. Stoll. H. Preuss, Theor. Chim. Acta 85 (1993) 441.

[22] F. Weigend. R. Ahlrichs, Phys. Chem. Chem. Phys. 7 (2005) 3297.

[23] F. Aquilante, J. Autschbach, R. K. Carlson, L. F. Chibotaru, M. G. Delcey, L. De Vico, I. F. Galván, N. Ferré, L. M. Frutos, L. Gagliardi, M. Garavelli, A. Giussani, C. E. Hoyer, G. L. Manni, H. Lischka, D. X. Ma, P. Malmqvist, T. Müller, A. Nenov, M. Olivucci, T. B. Pedersen, D. L. Peng, F. Plasser, B. Pritchard, M. Reiher, I. Rivalta, I. Schapiro, J. Segarra-Martí, M. Stenrup, D. G. Truhlar, L. Ungur, A. Valentini, S. Vancoillie, V. Veryazov, V. P. Vysotskiy, O. Weingart, F. Zapata, R. Lindh, J. Comput. Chem. 37 (2016) 506.

[24] B. O. Roos. P. R. Taylor. P. E. M. Siegbahn, Chem. Phys. 48 (1980), 157.

[25] P. A. Malmqvist. B. O. Roos. B. Schimmelpfennig, Chem. Phys. Lett. 357 (2002) 230.

[26] P. A. Malmqvist. B. O. Roos, Chem. Phys. Lett. 155 (1989) 189.

[27] L. F. Chibotaru. L. Ungur. J. Chem. Phys. 137 (2012) 064112.

[28] L. F. Chibotaru. L. Ungur. A. Soncini, Angew. Chem. Int. Ed. 47 (2008) 4126.

[29] L. Ungur, W. Van den Heuvel, L. F. Chibotaru, New J. Chem. 33 (2009) 1224.

[30] F. Aquilante. P.-A. Malmqvist. T.-B. Pedersen. A. Ghosh. B. O. Roos, J. Chem. Theory Comput. 4 (2008) 694.

[31] B. O. Roos. R. Lindh. P.-A. Malmqvist. V. Veryazov. P.-O. Widmark. J. Phys. Chem. A 108 (2004) 2851.

[32] B. O. Roos. R. Lindh. P.-A. Malmqvist. V. Veryazov. P.-O. Widmark. J. Phys. Chem. A 109 (2005) 6575.

[33] B. O. Roos. R. Lindh. P.-A. Malmqvist. V. Veryazov. P.-O. Widmark. A.-C. Borin. J. Phys. Chem. A 112 (2008) 11431.

[34] G. Laura, L. Roland, K. Gunnar, J. Chem. Phys. 121 (2004) 4494.

[35] G. Hung, G. Fernandez Garcia, I. Badlane, M. Camarra, S. Freslon, O. Guillou, C. Daiguebonne, F. Totti, O. Cador, T. Guizouarn, B. Le Guennic, K. Bernot, Chem. - Eur. J. 24 (2018) 6983.

[36] M. Feng, S. Speed, F. Pointillart, B. Lefeuvre, B. Le Guennic, S. Golhen, O. Cador, L. Ouahab, Eur. J. Inorg. Chem. (2016) 2039.

[37] M. Llunell, D. Casanova, J. Cirera, J. M. Bofill, P. Alemany, S. Alvarez, S. SHAPE (version 2.1), Barcelona, 2013.

[38] J. Wu, N. Dupont, S.-X. Liu, A. Neels, A. Hauser, S. Decurtins, Chem. Asian. J. 4 (2009) 399.

[39] O. Kahn, Molecular Magnetism, Wiley-VCH, Weinhem, Germany, 1993.

[40] J. M. Zadrozny, M. Atanasov, A. M.; Bryan, C.-Y. Lin, B. D. Rekken, P. P. Power, F. Neese, J. R. Long, Chem. Sci. 4 (2013) 125.

[41] (a) C. Dekker, A. F. M. Arts, H. W. de Wijn, A. J. van Duyneveldt, J. A. Mydosh, Phys. Rev. B: Condens. Matter Mater. Phys. 40 (1989) 11243; (b) J. Tang, P. Zhang, Lanthanide Single Molecule Magnets; Springer- Verlag: Berlin, 2015.

[42] K. Zhang, V. Montigaud, O. Cador, G. P. Li, B. Le Guennic, J. Tang, Y. Y. Wang Inorg. Chem. 57 (2018) 6983.

For Table of Contents Only

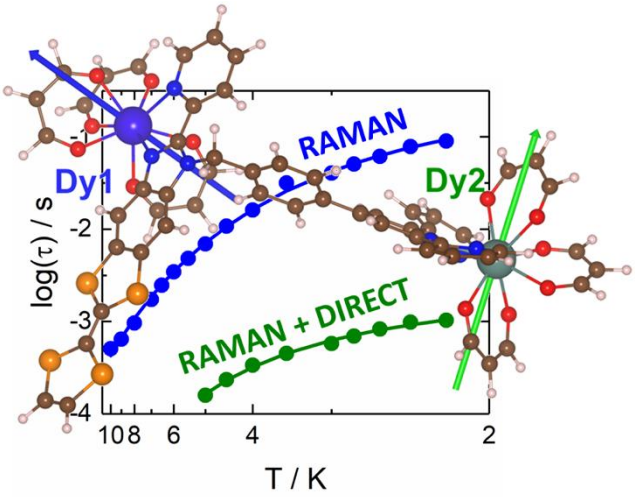

The Dy2 dinuclear complex behaves as a multi-field-induced Single-Molecule Magnet in which the two Ising Dy(III) ions display distinct relaxation times of their magnetization due to different magnetic relaxation processes.